Space-Time Adaptive Processing by Employing Structure-Aware Two-Level Block Sparsity

Zhizhuo Jiang, Xueqian Wang, *Member, IEEE*, Gang Li, *Senior Member, IEEE*, Xiao-Ping Zhang, *Fellow, IEEE*, and You He

***Abstract*—Traditional radar space-time adaptive processing (STAP) cannot efficiently suppress heterogeneous clutter because of a small number of independent and identically distributed training snapshots. In the article, we propose a new STAP approach exploiting structure-aware two-level block sparsity (STBS) of radar echoes, namely STBS-STAP. It enhances the performance on clutter suppression and target detection with limited training snapshots. The clutter angle-Doppler profile always appears in a continuous diagonal clustering structure and the radar echoes at the adjacent range cells commonly share the same sparse pattern. STBS-STAP employs STBS, i.e., both the diagonal clustering structure and the common sparsity property, to acquire a precise clutter covariance matrix estimation. Thus, the new STBS-STAP achieves better performance on clutter suppression compared with existing STAP methods with a small number of training samples. Besides, STBS-STAP achieves superior target detection performance due to the precise estimation of the statistical properties of the clutter. The superiority of STBS-STAP is verified by experiments on both simulated data and measured Mountain-Top data.**

***Index Terms*—Block sparsity, radar clutter suppression, space-time adaptive processing (STAP), structure-aware two-level block sparsity-based STAP (STBS-STAP).**

I. Introduction

AS ONE of the main tasks of airborne radars, target detection needs high signal-to-clutter-plus-noise ratio (SCNR) [1], [2]. However, the radar echoes of targets are usually much weaker than those of clutter contributions. It may significantly deteriorate the target detection performance if the clutter is not suppressed [3], [4].

Manuscript received June 30, 2020; revised February 28, 2021; accepted June 6, 2021. Date of publication June 23, 2021; date of current version July 14, 2021. This work was supported in part by the National Natural Science Foundation of China under Grants 61790551 and 61925106, in part by the Post-doctoral Innovative Talent Support Program under Grant BX20200195, in part by the China Postdoctoral Science Foundation under Grant 2020M680561, and in part by the Shuimu Tsinghua Scholar Program. This paper was presented in part at the IEEE Radar Conference, Boston, MA, USA, April 2019. *(Corresponding author: Gang Li.)*

Zhizhuo Jiang, Xueqian Wang, and Gang Li are with the Department of Electronic Engineering, Tsinghua University, Beijing 100084, China (e-mail: jzz16@mails.tsinghua.edu.cn; wangxueqian@mail.tsinghua.edu.cn; gangli@tsinghua.edu.cn).

Xiao-Ping Zhang is with the Department of Electrical, Computer and Biomedical Engineering, Ryerson University, Toronto, ON M5B 2K3, Canada (e-mail: xzhang@ee.ryerson.ca).

You He is with the Research Institute of Information Fusion, Naval Aviation University, Yantai 264001, China, and also with the Department of Electronic Engineering, Tsinghua University, Beijing 100084, China (e-mail: heyou_f@126.com).

Digital Object Identifier 10.1109/JSTARS.2021.3090069

Space-time adaptive processing (STAP) is an efficient technique to suppress clutter in the airborne radar and has been investigated more than a few decades [6], [7]. STAP can provide a significant SCNR increase in strong clutter environments, and it is beneficial to the subsequent target detection [8]–[14]. In other words, the better the clutter suppression performance of STAP is, the more benefits the subsequent detector gets.

For STAP techniques, it is essential to obtain the clutter covariance matrix (CCM) estimation by utilizing target-free training snapshots, which need to be independent and identically distributed (IID) [15]. The clutter suppression performance is decided by the precision of the estimated CCM, which depends on the quantity of IID training snapshots in the conventional STAP methods.

Assume that there are N array elements in the radar system, M pulses are received in a coherent processing interval (CPI). It has been proven that at least $2MN$ IID training samples are needed for the sample matrix inversion (SMI) method to guarantee its SCNR loss is not larger than 3dB in comparison with the optimal performance [15]. In heterogeneous clutter environments, the quantity of IID training snapshots may be limited.

Several partially-adaptive STAP approaches have been proposed to tackle the problem of a small number of training samples. The diagonal loaded SMI (LSMI) STAP method can achieve the near-optimal performance with only $2P$ training samples [16], [17], where $P \ll MN$ represents the quantity of interfering sources. Besides, the required quantity of training snapshots is reduced to twice of clutter rank while maintaining good performance in rank-reduction methods, e.g., the multistage Wiener filter [18]. However, the rank-reduction approaches are sensitive to the rank parameter. An inappropriate rank selection will cause the performance loss on clutter suppression.

Sparse property of the radar echoes has been employed in STAP techniques [19]–[24] to enhance the performance on clutter suppression with limited training samples. In [19], two different sparsity-based approaches are proposed to estimate CCM by leveraging the low-rank and sparse-structure properties. In [20], a sparsity-based STAP method using orthogonal frequency division multiplexing waveform significantly reduces the quantity of training snapshots without sacrificing the performance on clutter suppression. In [21], Wang *et al.* developed a STAP method to obtain the clutter subspace with fewer training samples by utilizing the sparsity of the signal. In [23], based on subspace tracking, a fast sparsity-based STAP method is developed, it improves the robustness in clutter subspace estimation due to

the utilization of the low-rank information of CCM. In [24], to reduce the effect of gain/phase errors, the authors reformulate the STAP problem by a joint optimization issue and develop a robust approach to eliminate the clutter.

The block sparsity is employed for existing sparsity-based approaches to improve the estimation accuracy of sparse signals. According to existing literatures, the two categories of applications of the block sparsity are summarized as follows.

1) *Common Sparsity*: it is called the model of multiple measurement vectors (MMVs) as well [25]–[30]. The positions of dominant elements of the multiple signals are almost the same in MMV models. In [25], a STAP method based on sparse Bayesian learning using multiple training samples is proposed and achieves satisfactory clutter suppression performance with fast implementation. In [29] and [30], Sun *et al*.derived two sparsity-based methods to obtain the clutter profile in the angle-Doppler domain (i.e., the clutter angle-Doppler profile). The common sparsity is used in the methods to eliminate the pseudo-peaks appearing at different range cells.
2) *Clustering Property*: It is also referred to as group sparsity [31]–[34]. The clustering property can be employed to effectively reconstruct the group sparse signals, in which the nonzero entries have a clustered structure. The typical algorithms based on group sparsity include the group Lasso (GLASSO) [31], the block orthogonal matching pursuit [32], and the sparse recovery with Markov random field (MRF) [34].

However, existing sparsity-based STAP approaches only utilize one of the two kinds of the block-sparsity properties. Note that in [35]–[37], several methods based on hierarchical Bayesian framework are proposed to reduce the recovery error of the sparse signals by employing two kinds of block sparsity. In [38], the two kinds of block-sparsity properties are fused to enhance the imaging quality of polarimetric through-wall radar. This implies that the two kinds of the block sparsity contain different types of information of sparse signals. They can be utilized together to further reduce the estimation error of the sparse vectors. However, the clustering property employed in [35]–[38] does not contain any spatial structure information about the sparse signals.

It is well known that in the angle-Doppler domain (of the STAP application), a clutter ridge is observed according to the coupling of the spatial dimension and the Doppler dimension. Therefore, the clutter is presented as the special diagonal clustering structure when the array is in the side-looking configuration, leading to the block sparsity of the clutter angle-Doppler profile. Meanwhile, the radar echoes at the adjacent range cells commonly share the same sparse pattern. In other words, the common sparsity pattern still exists at the adjacent range cells in STAP applications.

In the article, a new STAP algorithm by exploiting structure-aware two-level block sparsity (STBS), referred to as STBS-STAP, is proposed. In the new STBS-STAP, an MRF [39] is employed to describe the dependence between a support index and its neighbors. Specifically, the weighted eight-neighbor strategy based on the MRF is designed to capture the diagonal clustering structure in the angle-Doppler domain. Then, we modify the smooth Gaussian function to capture the contribution of the common sparsity. In general, STBS-STAP combines the special diagonal clustering structure and the common sparsity to acquires more accurate clutter angle-Doppler profile and subsequent CCM.

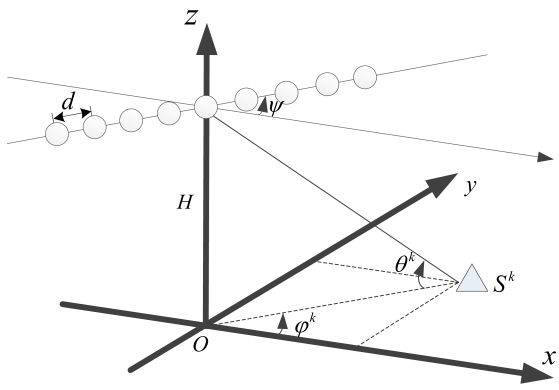

Fig. 1. Observed scene of airborne STAP radar.

As a result of obtaining an accurate CCM estimation, the new STBS-STAP outperforms existing STAP methods in terms of the performance on clutter suppression and target detection based on limited training snapshots.

It should be noted that the basic concept of two-level block sparsity in STAP applications is proposed in our previous conference paper [5]. On top of [5], the model of two-level block sparsity is significantly improved to enforce the diagonal clustering structure of the clutter profile. New derivation of STBS-STAP is given and its extensive analyses are conducted. The superiority of the new STBS-STAP over existing STAP methods is demonstrated with extensive experiments based on both simulated data and measured Mountain-Top data.

We also note that, the sparsity-based STAP has been recently extended to various application scenarios, such as: STAP in the extremely heterogeneous environment where only one training sample is available [40], [41], STAP for different radar system [42]–[45], and STAP methods to solve the problem of off-grid [46]–[48]. The optimization problems in [40]–[48] are different from that in this article since here we focus on the performance improvement of clutter suppression and target detection for the ordinary airborne radar via the STBS when a few training samples are available. Therefore, the methods in these papers are not applied to evaluate the performance of the proposed STBS-STAP.

The rest of this article is organized as follows. In Section II, the signal model is reviewed. In Section III, the STBS for STAP applications is formulated and STBS-STAP is proposed. The performance and running time of STBS-STAP are assessed by experiments based on simulated data and measured data in Section IV. Conclusion is given in Section V.

II. Signal Model

The observed scene of an airborne radar system is illustrated in Fig. 1 [49]. The aircraft flies in the x-direction. H and v represent the height and the velocity of this aircraft, respectively. We use d to denote the inter-channel spacing. The triangle S^k denotes

the kth clutter scatterer. ψ stands for the crab angle as shown in Fig. 1. In this article, $\psi = 0$ is assumed, i.e., the side-looking configuration is considered.

The clutter component is modeled as the superposition of N_c clutter scatterers for each range cell. For the kth clutter scatterer, the azimuth angle is denoted as φ_c^k, $\theta_c^k$is the elevation angle. The normalized Doppler frequency $f_{d,c}^k$ and spatial frequency $f_{s,c}^k$ corresponding to the kth clutter scatterer are described as [27]

$$f_{d,c}^k = \frac{2v}{\lambda f_r}\cos\varphi_c^k cos\theta_c^k$$
$$f_{s,c}^k = \frac{d}{\lambda}\cos\varphi_c^k cos\theta_c^k \tag{1}$$

for $k = 1, 2, \ldots, N_c$. In (1), λ and f_r denote the wavelength and the pulse repetition frequency (PRF), separately. The superscript of k is the index of the clutter scatterer, the subscript c, d, and s denote the clutter, the Doppler dimension and the spatial dimension, respectively.

Suppose that the radar system consists of N array elements, M pulses are received in a CPI. The space-time steering vector corresponding to the k-th clutter scatterer is defined by

$$\boldsymbol{v}\left(f_{d,c}^k, f_{s,c}^k\right) = \boldsymbol{v}_d\left(f_{d,c}^k\right) \otimes \boldsymbol{v}_s\left(f_{s,c}^k\right) \tag{2}$$

where $\otimes$ denotes the operator of Kronecker product, $\boldsymbol{v}_d(f_{d,c}^k) = [1, \exp(j2\pi f_{d,c}^k), \ldots, \exp(j2\pi(M-1)f_{d,c}^k)]^T$ is the $M \times 1$ temporal steering vector, $\boldsymbol{v}_s(f_{s,c}^k) = [1, \exp(j2\pi f_{s,c}^k), \ldots, \exp(j2\pi(N-1)f_{s,c}^k)]^T$ stands for the $N \times 1$ spatial steering vector. Then for the lth range cell, the received clutter plus noise is described [24]

$$\boldsymbol{x}^{(l)} = \boldsymbol{x}_c^{(l)} + \boldsymbol{x}_n^{(l)} = \sum_{k=1}^{N_c} \alpha_c^k \boldsymbol{v}\left(f_{d,c}^k, f_{s,c}^k\right) + \boldsymbol{x}_n^{(l)} \tag{3}$$

where α_c^k is the complex reflectivity corresponding to the kth clutter scatterer, $\boldsymbol{x}_n^{(l)}$ denotes the Gaussian noise. The subscript n represents the noise. The superscript of l represents the index of the range cell.

By discretizing the angle-Doppler domain into $N_s \times N_d$ grids, where N_s and N_d denote the discretized size of the spatial dimension and Doppler dimension, respectively. (3) is rewritten as

$$\boldsymbol{X} = \boldsymbol{\Psi}\boldsymbol{\Theta} + \boldsymbol{B} \tag{4}$$

where $\boldsymbol{X} = [\boldsymbol{x}^{(1)}, \boldsymbol{x}^{(2)}, \ldots, \boldsymbol{x}^{(L)}]$ denotes the $NM \times L$ training snapshot matrix, L denotes the quantity of training snapshots, $\boldsymbol{\Theta} = [\boldsymbol{\theta}^{(1)}, \boldsymbol{\theta}^{(2)}, \ldots, \boldsymbol{\theta}^{(L)}] \in \mathbb{C}^{N_d N_s \times L}$ represents the clutter profile matrix, $\boldsymbol{B} = [\boldsymbol{b}^{(1)}, \boldsymbol{b}^{(2)}, \ldots, \boldsymbol{b}^{(L)}] \in \mathbb{C}^{N_d N_s \times L}$ refers to the complex Gaussian noise matrix where the mean is zero. Note that we use K to denote the clutter sparsity of $\boldsymbol{\theta}^{(l)}$. $\boldsymbol{\Psi} \in \mathbb{C}^{NM \times N_d N_s}$ with $NM < N_s N_d$ represents the overcomplete dictionary. Specifically, $\boldsymbol{\Psi}$ consists of all these space-time steering vectors in the angle-Doppler domain, expressed as

$$\boldsymbol{\Psi} = \left[\boldsymbol{v}\left(f_d^1, f_s^1\right), \ldots, \boldsymbol{v}\left(f_d^1, f_s^{N_s}\right), \ldots \right.$$
$$\left. \boldsymbol{v}\left(f_d^{N_d}, f_s^1\right), \ldots \boldsymbol{v}\left(f_d^{N_d}, f_s^{N_s}\right)\right]. \tag{5}$$

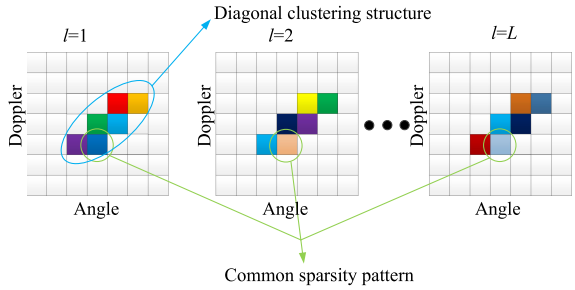

Fig. 2. Intuitive representation of the STBS in the range-angle-Doppler domain. The colorized lattice represents the clutter area, while the white lattice means the nonclutter area. In the angle-Doppler domain, the clutter presents a special diagonal clustering structure. Across the adjacent range cells, the clutter profiles share the common sparsity pattern.

When the clutter profile estimation $\{\hat{\boldsymbol{\theta}}^{(l)} | l = 1, 2, \ldots, L\}$ are acquired, the estimated CCM is obtained from [19], [27], [50]

$$\hat{\boldsymbol{R}} = \sum_{i=1}^{N_d N_s} \left|\hat{\boldsymbol{\theta}}_i\right|^2 \boldsymbol{v}\left(f_d^i, f_s^i\right) \boldsymbol{v}\left(f_d^i, f_s^i\right)^H + \sigma^2 \boldsymbol{I} \tag{6}$$

where $(\cdot)^H$ and $|\cdot|$ denote the operators of conjugate transpose and modulus, respectively. $|\hat{\boldsymbol{\theta}}_i|^2 = \frac{1}{L}\sum_{l=1}^{L} |\hat{\boldsymbol{\theta}}_i^{(l)}|^2$, where $\hat{\boldsymbol{\theta}}_i^{(l)}$ is the ith entry of the clutter profile estimation corresponding to the training snapshot. $\boldsymbol{I}$ is the identity matrix, σ^2 is a small loading parameter which represents the noise level. Note that the accuracy of $\hat{\boldsymbol{R}}$ is decided by the accuracy of the clutter profile estimation $\hat{\boldsymbol{\theta}}_i$. In the light of the minimum noise variance principle, the STAP filter is acquired from the problem

$$\min_{\boldsymbol{w}} \boldsymbol{w}^H \hat{\boldsymbol{R}} w \text{ s.t. } \boldsymbol{w}^H \boldsymbol{v}_t\left(f_{d,t}, f_{s,t}\right) = 1 \tag{7}$$

where $f_{d,t}$ denotes the normalized Doppler frequency, $f_{s,t}$ is normalized spatial frequency of the target, respectively. The subscript t represents the target. $\boldsymbol{v}_t(f_{d,t}, f_{s,t})$ denotes the target steering vector. The STAP weight vector is calculated [46], [51]

$$\hat{\boldsymbol{w}} = \frac{\hat{\boldsymbol{R}}^{-1}\boldsymbol{v}_t\left(f_{d,t}, f_{s,t}\right)}{\boldsymbol{v}_t\left(f_{d,t}, f_{s,t}\right)^H \hat{\boldsymbol{R}}^{-1} \boldsymbol{v}_t\left(f_{d,t}, f_{s,t}\right)}. \tag{8}$$

III. Proposed STAP Algorithm Based on STBS

In this section, the STBS in the STAP application is first formulated. Then, the corresponding STAP algorithm, namely STBS-STAP, is proposed.

A. Formulation of the STBS in STAP Applications

An intuitive representation of STBS for STAP applications is presented in Fig. 2 in the range-angle-Doppler domain. In the angle-Doppler domain, there exists the clutter ridge because of the movement of the aircraft. Thus, it is an inherent property that the clutter profile presents a special diagonal clustering structure when the array is in a side-looking configuration. The diagonal clustering structure is considered as a kind of the block sparsity [52]. Besides, at the adjacent range cells, the clutter profiles share the common sparsity pattern, namely another kind of the block sparsity.

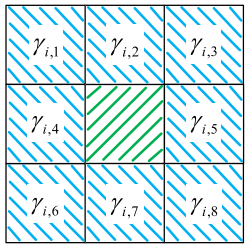

Fig. 3. Illustration of the weight of interaction. The green shaded lattice denotes the support index under test and the blue shaded lattices are its 8 neighbors.

In the following, we formulate the STBS of clutter profiles in detail.

1) In the angle-Doppler domain, the clutter appears in a special diagonal clustered sparse fashion.*:* We denote the set of indices of the nonzero elements of $\boldsymbol{\theta}^{(l)}$ as the support set $\Lambda^{(l)}$, namely, $\Lambda^{(l)}$ contains positions corresponding to the clutter component in $\boldsymbol{\theta}^{(l)}$. We use $\bar{\Lambda}^{(l)}$, namely the complementary set of $\Lambda^{(l)}$ to denote support set corresponding to nonclutter area in $\boldsymbol{\theta}^{(l)}$. An indicator vector $\boldsymbol{\tau} \in \mathbb{Z}^{N_d N_s \times 1}$ is defined to signify whether the clutter area contains the support index i, and $\boldsymbol{\tau}$ is composed of 1 and -1, i.e., $\boldsymbol{\tau}_{\Lambda^{(l)}} = \mathbf{1}$ and $\boldsymbol{\tau}_{\bar{\Lambda}^{(l)}} = -\mathbf{1}$.

The MRF is an efficient tool to measure the interaction between the support index and its neighbors [39], [53] and has been widely used in ISAR imaging [53] and target detection [54]. Here, the MRF is employed to measure the diagonal clustering property of the clutter angle-Doppler profile. Specifically, the interaction between the support index and its neighbors captured by the MRF is described by [39]

$$p\left(\tau_i \middle| \boldsymbol{\tau}_{N_i}\right) \propto \exp\left(\sum_{j \in N_i} \gamma_{i,j} \tau_i \tau_j\right) \tag{9}$$

where N_i denotes the set of eight-neighbor for the support index *i*, $\{\gamma_{i,j}, \forall j \in N_i\}$ is the weight of interaction between the support index *i* and its neighbor *j*.

In STAP applications, different from the clustering pattern employed in through-wall radar imaging applications such as in [38], the clustering property of the clutter angle-Doppler profile is identified as a special pattern, i.e., the diagonal clustering structure. As such, the weighted eight-neighbor strategy based on the MRF for $\{\gamma_{i,j}, \forall j \in N_i\}$ is designed to enhance the diagonal clustering property. Note that the weighted eight-neighbor strategy is one of the variants of the second-order neighborhood system in [53]. The illustration of $\{\gamma_{i,j}, \forall j \in N_i\}$ is shown in Fig. 3.

For a support index *i*, the values of $\{\gamma_{i,j}, \forall j \in N_i\}$ are assigned by solving the following formulas:

$$\begin{cases} \sum_{j \in N_i} \gamma_{i,j} = 1 \\ \gamma_{i,j} \geq 0, \forall j \in N_i \\ \gamma_{i,3} = \gamma_{i,6} > \gamma_{i,1} = \gamma_{i,2} = \gamma_{i,4} = \gamma_{i,5} = \gamma_{i,7} = \gamma_{i,8} \end{cases}. \tag{10}$$

The first equation limits the overall weight from the neighbors of the support index *i*, the second formula defines that the weights are nonnegative, and the relationship between weights are illustrated by the last formula. Specifically, we empirically set $\gamma_{i,6} = 2\gamma_{i,1}$. It means that in the eight neighbors of the support index *i,* the weights of diagonal support indices are twice as large as those of nondiagonal support indices. Here, we introduce weight ratio to denote the ratios of weights of diagonal neighbors to those of nondiagonal neighbors. Therefore, the weight ratio is 2 here. Then, we can have $\gamma_{i,j} = \begin{cases} 0.2, j = 3, 6 \\ 0.1, j = 1, 2, 4, 5, 7, 8 \end{cases}$. Apparently, the weighted eight-neighbor strategy utilizes more information than the first-order neighborhood system in [55], [56].

2) At adjacent range cells, the clutter angle-Doppler profiles possess a similar sparse pattern, i.e., the common sparsity [57]. As shown in Fig. 2, the common sparsity at the adjacent range cells illustrates that the support set of nonzero elements of $\boldsymbol{\theta}^{(l)}$ is supposed to be identical for $l = 1, 2, \ldots, L$, while the dominant entries of $\boldsymbol{\theta}^{(l)}$ may change for different $l = 1, 2, \ldots, L$. In the light of the common sparsity across multiple clutter profiles, we use Λ_{comm} to denote the common support set. It means $\Lambda_{\text{comm}} = \Lambda^{(l)}$ for $l = 1, 2, \ldots, L$, and accordingly $\boldsymbol{\tau}_{\Lambda_{\text{comm}}} = \mathbf{1}$ and $\tau_{\bar{\Lambda}_{\text{comm}}} = -\mathbf{1}$. The subscript $comm$ denotes the common sparsity.

Here, we focus on the selection of the support indices of the clutter component, namely the support set Λ which satisfies $\boldsymbol{\tau}_{\Lambda} = \mathbf{1}$. When Λ is identified, the accurate estimation of the clutter angle-Doppler profile $\hat{\boldsymbol{\theta}}$ is accordingly acquired by performing the least squares approach. It also means that the support set Λ, which satisfies both diagonal clustering property and common sparsity, is vital to the CCM estimation and the subsequent clutter suppression.

Same as in [38], we employ the probabilistic graph model developed in [58], [59] to combine the two kinds of block sparsity. Then, we describe the relationship between $\{\boldsymbol{\theta}^{(1)}, \boldsymbol{\theta}^{(2)}, \ldots, \boldsymbol{\theta}^{(L)}\}$, τ_i and $\boldsymbol{\tau}_{N_i}$ as a joint distribution

$$p\left(\theta_i^{(1)}, \ldots, \theta_i^{(L)}, \tau_i, \boldsymbol{\tau}_{N_i}\right) \propto p\left(\tau_i \middle| \boldsymbol{\tau}_{N_i}\right) \prod_{l=1}^{L} p\left(\theta_i^{(l)} \middle| \tau_i\right). \tag{11}$$

By maximizing the above joint distribution, the estimation of τ_i is obtained by:=

$$\begin{cases} \hat{\tau}_i = 1, \varepsilon_i > \beta \\ \hat{\tau}_i = -1, \varepsilon_i \leq \beta \end{cases} \tag{12}$$

where

$$\varepsilon_i = 2 \sum_{j \in N_i} \gamma_{i,j} \tau_j + \sum_{l=1}^{L} \log\left[p\left(\theta_i^{(l)} \middle| \tau_i = 1\right) \Big/ p\left(\theta_i^{(l)} \middle| \tau_i = -1\right)\right]. \tag{13}$$

Instead of setting $\beta = 0$ as in [38], in this article, the threshold β is determined by an adaptive approach to meet the requirement of the clutter sparsity of $\boldsymbol{\tau}$ and will be shown in Section III-B.

Next, we indicate the relationship between the clutter profile $\boldsymbol{\theta}^{(l)}$ and indicator vector $\boldsymbol{\tau}$ and measure the contribution of the common sparsity. Note that $\theta_i^{(l)}$ presents a nonzero coefficient

when $\tau_i = 1$ and tends to be a zero value when $\tau_i = -1$. To reduce the parameters of the approximation function in [38], we introduce and modify a smooth Gaussian function to approximate the contribution of the common sparsity, i.e.,

$$\sum_{l=1}^{L} \log \left[p\left(\theta_i^{(l)} \middle| \tau_i = 1\right) \Big/ p\left(\theta_i^{(l)} \middle| \tau_i = -1\right) \right]. \tag{14}$$

The modified smooth Gaussian function is defined by

$$f\left(\theta_i^{(l)}\right) = \rho \left[1 - 2\exp\left(-\frac{\theta_i^{(l)} \left(\theta_i^{(l)}\right)^*}{2\delta^2} \right) \right] \tag{15}$$

where $(\cdot)^*$denote the operators of conjugate. It is approximately given by

$$f\left(\theta_i^{(l)}\right) = \begin{cases} \rho, & \left|\theta_i^{(l)}\right| \gg \delta \\ -\rho, & \left|\theta_i^{(l)}\right| \ll \delta \end{cases} \tag{16}$$

where ρ is the scale parameter to balance the diagonal clustering pattern and common sparsity in STBS. It is empirically set to $0.2/L$ according to the value of $\gamma_{i,j}$ in (10). δ is the only parameter to determine the quality of approximation. It is determined by an adaptive approach that is defined by (20) in the next subsection. Then, (13) is rewritten as

$$\varepsilon_i = \varepsilon_{i,\mathrm{clus}} + \varepsilon_{i,\mathrm{comm}} \tag{17}$$

where

$$\varepsilon_{i,\mathrm{clus}} = 2 \sum_{j \in N_i} \gamma_{i,j} \tau_j \tag{18}$$

$$\varepsilon_{i,\mathrm{comm}} = \sum_{l=1}^{L} f\left(\theta_i^{(l)}\right). \tag{19}$$

In (17), $\varepsilon_{i,\mathrm{clus}}$ captures the contribution of the eight-neighbor support set, i.e., the special diagonal clustering structure. The subscript $clus$ denotes the clustering property. $\varepsilon_{i,\mathrm{comm}}$ denotes the contribution of the common sparsity. Meanwhile, the weighted eight-neighbor strategy, i.e., the employment of $\{\gamma_{i,j}, \forall j \in N_i\}$ enhances the diagonal clustering property of the clutter angle-Doppler profile. In other words, both the two kinds of block-sparsity properties are considered in ε_i and they are fused to determine $\tau_i = 1$ or $\tau_i = -1$.

B. New STBS Based STAP Algorithm

In this section, we propose a new STAP approach (STBS-STAP) by employing the STBS. The new STBS-STAP enhances the performance on clutter suppression based on a small number of training snapshots. It combines the common sparsity and the special diagonal clustering structure to acquire the accurate CCM estimation.

In Algorithm 1, we elaborate the steps of STBS-STAP and describe it in Algorithm 1.

The dictionary matrix $\boldsymbol{\Psi}$ in (4) is coherent in STAP applications [51] and the SSCoSaMP(L1) approach is robust to the coherence between columns of the dictionary matrix [60].

Algorithm 1: STBS-STAP.

Input: $\{\boldsymbol{x}^{(l)} | l = 1, 2, \ldots, L\}, \boldsymbol{\Psi}, K$.
Initialization: $\boldsymbol{\theta}^{(l)} = \mathbf{0}^{N_d N_s \times 1}$, for $l = 1, 2, \ldots, L$.
1: $\Lambda^{(l)} = \mathrm{SSCoSaMP(L1)}(\boldsymbol{x}^{(l)}, K)$, for $l = 1, 2, \ldots, L$.
2: $\Lambda_{\mathrm{vote}} = \mathrm{vote}(\{\Lambda^{(l)} | l = 1, 2, \ldots, L\}, K)$, where $\mathrm{vote}(\{\Lambda^{(l)} | l = 1, 2, \ldots, L\})$ obtains the collection of *K* elements that possess the highest scores in the light of their appearance in $\{\Lambda^{(l)} | l = 1, 2, \ldots, L\}$.
3: set $\boldsymbol{\tau}_{\Lambda_{\mathrm{vote}}} = \mathbf{1}, \boldsymbol{\tau}_{\bar{\Lambda}_{\mathrm{vote}}} = -\mathbf{1}$ and calculate $\breve{\boldsymbol{\theta}}^{(l)}_{\Lambda_{\mathrm{vote}}} = (\boldsymbol{\Psi}_{\Lambda_{\mathrm{vote}}})^{\dagger} \boldsymbol{x}^{(l)}$ for $l = 1, 2, \ldots, L$.
4: compute ε_i in (17) by using $\{\breve{\boldsymbol{\theta}}^{(1)}, \breve{\boldsymbol{\theta}}^{(2)}, \ldots, \breve{\boldsymbol{\theta}}^{(L)}\}$ and $\boldsymbol{\tau}_{N_i}$ for $i \in \{1, 2, \ldots, N_d N_s\}$, if $\varepsilon_i > \beta$, $\hat{\tau}_i = 1$, else $\hat{\tau}_i = -1$.
5: $\Lambda_{\mathrm{new}} =$ {the set of positions which correspond to '1' in $\hat{\boldsymbol{\tau}}$}.
6: $\hat{\boldsymbol{\theta}}^{(l)}_{\Lambda_{\mathrm{new}}} = (\boldsymbol{\Psi}_{\Lambda_{\mathrm{new}}})^{\dagger} \boldsymbol{x}^{(l)}$, then the smallest $N_d N_s - K$ coefficients of $\hat{\boldsymbol{\theta}}^{(l,new)}$ are forced to be zeros, for $l = 1, 2, \ldots, L$.
Output: $\hat{\boldsymbol{\theta}}^{(l)}_{\Lambda_{\mathrm{new}}}$, for $l = 1, 2, \ldots, L$.

Therefore, SSCoSaMP(L1) is utilized to acquire the temporary support sets $\{\Lambda^{(l)} | l = 1, 2, \ldots, L\}$ corresponding to the clutter area in step 1. In step 2, to combine the information of multiple range cells and eliminate the effect of the measurement noise, the voting support set Λ_{vote} is obtained by the operation of voting. Λ_{vote} obtains the collection of *K* elements with the highest scores according to their appearance in $\{\Lambda^{(l)} | l = 1, 2, \ldots, L\}$ [5], [61]. Subsequently, the indicator vector $\boldsymbol{\tau}$ is set to $\boldsymbol{\tau}_{\Lambda_{vote}} = \mathbf{1}$ and $\boldsymbol{\tau}_{\bar{\Lambda}_{\mathrm{vote}}} = -\mathbf{1}$ in step 3. By performing the least squares approach, we obtain the temporary estimation $\breve{\boldsymbol{\theta}}^{(l)}_{\Lambda_{\mathrm{vote}}} = (\boldsymbol{\Psi}_{\Lambda_{\mathrm{vote}}})^{\dagger} \boldsymbol{x}^{(l)}$, where $(\cdot)^{\dagger}$ denotes the operation of pseudoinverse.

Step 4 is the key part of the new algorithm. Based on $\{\breve{\boldsymbol{\theta}}^{(1)}, \breve{\boldsymbol{\theta}}^{(2)}, \ldots, \breve{\boldsymbol{\theta}}^{(L)}\}$ and $\boldsymbol{\tau}_{N_i}$, we calculate ε_i in (17) by combining the diagonal clustering property and common sparsity. Then we determine the indicator vector in (12) for $i \in \{1, 2, \ldots, N_d N_s\}$. The employment of the common sparsity reduces the influence of the measurement noise. The utilization of the diagonal clustering property decreases the required number of training samples. The support indices that satisfy both clustering property and common sparsity are selected. Note that the parameter δ and β in (16) and (12) are adaptively determined by

$$\begin{aligned} \delta &= \mathrm{thre\_ind}\left(\breve{\boldsymbol{\theta}}^{(l)}, K\right) \\ \beta &= \mathrm{thre\_ind}\left(\boldsymbol{\varepsilon}, K\right) \end{aligned} \tag{20}$$

where $\boldsymbol{\varepsilon} = [\varepsilon_1, \varepsilon_2, \ldots, \varepsilon_{N_d N_s}]$ and $\mathrm{thre\_ind}(\boldsymbol{z}, K)$ obtains the *K*th largest magnitude of the coefficients of $\boldsymbol{z}$

We select the support index i that satisfies $\boldsymbol{\tau}_i = 1$ to form the new support set Λ_{new} in step 5. Therefore, Λ_{new} is acquired by combining STBS. Then, we obtain the clutter profile estimation by performing the least squares approach with the new support set Λ_{new} in step 6. The smallest $N_d N_s - K$ entries of $\hat{\boldsymbol{\theta}}^{(l)}$ are forced to be zero to guarantee the sparsity of solutions.

In the following, we discuss the differences between STBS-STAP and existing methods.

1) STBS-STAP combines both the special diagonal clustering property and the common sparsity, while existing STAP methods based on SRMMV [30] and GLASSO [31] only utilize one of the two properties. Note that the two properties contain different types of information of sparse signals. Specifically, the employment of the common sparsity reduces the impact of the measurement noise. The diagonal clustering property is utilized to reduce the required training snapshots. Accordingly, STBS further enhances the performance on clutter suppression based on limited training snapshots in STAP applications.
2) Different from the two-level block sparsity employed for through-wall radar imaging in [38] and ISAR imaging [36], STBS-STAP enforces the special diagonal clustering structure of the clutter profile present in STAP applications. The weighted eight-neighbor strategy is employed to capture the continuous diagonal structure of the clutter ridge. As such, STBS-STAP can obtain a more precise support set corresponding to the clutter area, thereby improving the estimation accuracy of CCM. In addition, the contribution of common sparsity is captured by the modified smooth Gaussian function in STBS-STAP instead of step functions in [38]. It reduces the number of parameters that need to be tuned.
3) Unlike BOMP [32] and GLASSO [31] that need a vector of block partition in advance, STBS-STAP does not need the prior information of the block partition.

IV. Experimental Results

In the following, STBS-STAP is compared with state-of-the-art sparsity-based approach, such as MFCSBL [25], SRMMV [30], and GLASSO [31], and the classical LSMI method [16] in terms of the performance on clutter suppression and target detection by using the simulated data and measured Mountain-Top data.

A. Simulation Results

In this section, the improvement factor (IF) performances of different approaches are evaluated

$$\text{IF} = \frac{\left|\hat{\boldsymbol{w}}^H \boldsymbol{v}_t\left(f_{d,t}, f_{s,t}\right)\right|^2 \Big/ \hat{\boldsymbol{w}}^H \boldsymbol{R} \hat{\boldsymbol{w}}}{\boldsymbol{v}_t\left(f_{d,t}, f_{s,t}\right)^H \boldsymbol{v}_t\left(f_{d,t}, f_{s,t}\right) \Big/ tr\left(\boldsymbol{R}\right)} \tag{21}$$

where $\boldsymbol{R}$ represents the true clutter-plus-noise covariance matrix, and *tr* (.) denotes the trace operator. The IF value is defined as the SCNR improvement of radar echoes by using the STAP filter.

Assume a side-looking uniform linear array consists of 14 antenna elements where 16 pulses are received in a CPI. Other system parameters are listed as follows: PRF is 3000 Hz, wavelength is 0.2 m, the inter-channel spacing is half wavelength, the height and the velocity of the platform is 10 km and 150 m/s. The clutter-to-noise ratio (CNR) is 40 dB. In the simulation part, the clutter fluctuations are considered and modeled by the Gaussian model [62]. In this Gaussian model, the clutter bandwidth is set to 400 Hz. We discretize the angle-Doppler domain into $N_s = 48$ spatial bins and $N_d = 48$ Doppler bins. Besides, the added noise follows the complex Gaussian distribution.

For the proposed STBS-STAP, we set the clutter sparsity to $K = 40$. For GLASSO, the size of the block partition is 2. The loading factor in (6) is set to the noise power.

The true Capon spectrum of the clutter corresponding to the cell under test (CUT) is illustrated in Fig. 4(a). The estimated clutter profiles of STBS-STAP, SRMMV, GLASSO, and MFCSBL are depicted in Fig. 4(b)–(e) with 20 training samples. We normalize the maximum intensity value of all the clutter profiles to 0 dB, then the image intensity of the clutter profiles is plotted on a $[-20, 0]$ dB scale. It is shown in Fig. 4(b) that the clutter angle-Doppler profile estimated by STBS-STAP approximates the true Capon spectrum better. The reason is that the new STBS-STAP acquires precise support set of the clutter area by combining the common sparse pattern and the clustering property. In addition, the underlying diagonal clustering structure of the clutter profile is further enhanced by the designed weighted eight-neighbor strategy in STBS-STAP. With regard to the clutter profiles estimated by SRMMV and MFCSBL in Fig. 4(c) and (e), several superfluous nonzero coefficients exist. Besides, more support indices of the clutter ridge are missing in Fig. 4(e) compared with the true Capon spectrum. In Fig. 4(d), there are massive spurious entries in the clutter profile obtained by GLASSO.

In Fig. 5, the IF value in terms of the Doppler frequency is illustrated to evaluate different algorithms. The IF values are acquired by fixing the normalized spatial frequency to 0.26. We consider two cases in Fig. 5, i.e., $L = 8$ and $L = 20$. The optimal IF curve, referred to as OPT, is obtained when the true CCM is known. As shown in Fig. 5, STBS-STAP achieves superior IF performance. The IF value of STBS-STAP is closer to the optimal case than other methods even with eight training samples. It means that the radar echoes can obtain higher SCNR improvement after passing through the STAP filter formed by the new STBS-STAP. The reason is that the new STBS-STAP obtains more accurate estimation of the clutter profile by exploiting the property of the diagonal clustering structure and the common sparsity at the adjacent range cells, namely the STBS. MFCSBL yields poorer IF performance than STBS-STAP. Compared with STBS-STAP, the IF values of SRMMV and GLASSO are lower. The reason is that SRMMV and MFCSBL only take common sparsity into consideration and GLASSO only utilizes clustering property. The two properties contain different types of information of sparse signals. Therefore, the performances of MFCSBL, SRMMV, and GLASSO degrade due to the underutilization of block sparse information. In Fig. 5(b), the IF values of different methods are improved with 20 training snapshots. STBS-STAP

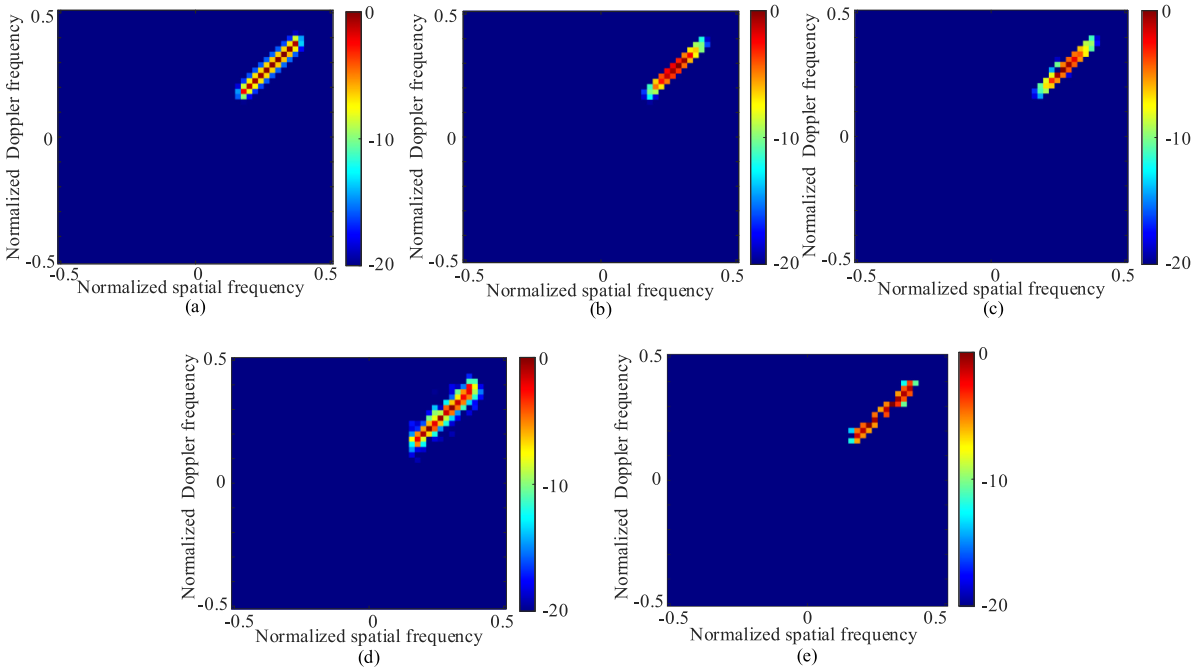

Fig. 4. True Capon spectrum and estimated clutter profile in the range CUT. (a) True Capon spectrum. (b) Estimated clutter profile using STBS-STAP. (c) Estimated clutter profile using SRMMV. (d) Estimated clutter profile using GLASSO (e) Estimated clutter profile using MFCSBL. The clutter profile estimated by STBS-STAP is closest to the true Capon spectrum. In Fig. 4(c) and (d), several superfluous nonzero coefficients in the clutter profiles exist. In Fig. 4(e), more support indices of the clutter ridge are missing.

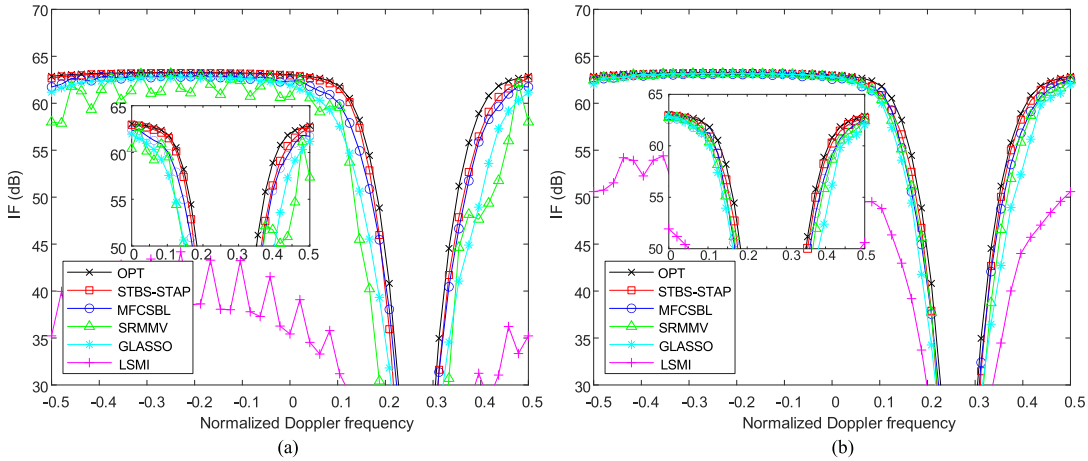

Fig. 5. IF curve comparison with (a) 8 training samples (b) 20 training samples. The IF performance of STBS-STAP is better than MFCSBL, SRMMV, GLASSO and LSMI.

also achieves superior IF performance. Besides, we find the IF performance of LSMI is unsatisfactory because of the severely lack of training samples.

In addition, it is illustrated in Fig. 5 that STBS-STAP acquires a narrower notch than MFCSBL, SRMMV, and GLASSO in the mainlobe clutter region. Intuitively, it achieves higher SCNR improvement after passing the STAP filter formed by STBS-STAP for targets that are close to the clutter ridge in the angle-Doppler domain. It means STBS-STAP provides the better detection performance even the targets are close to the clutter ridge. The reason is that STBS-STAP obtains more accurate support set estimation by employing STBS, leading to a more accurate CCM estimation. Therefore, the filter formed by STBS-STAP leads to better performance on the clutter suppression and the target detection.

Next, several simulations are conducted to illustrate the robustness of the new SBTS-STAP to related parameters. The IF values of STBS-STAP in terms of the weight ratio, the clutter sparsity and different CNR values are shown in Fig. 6 by using eight training samples. The parameters in these simulations are same as before. From Fig. 6(a), we find that the IF performance of STBS-STAP with weight ratios ranging from 1.5 to 2.5 is

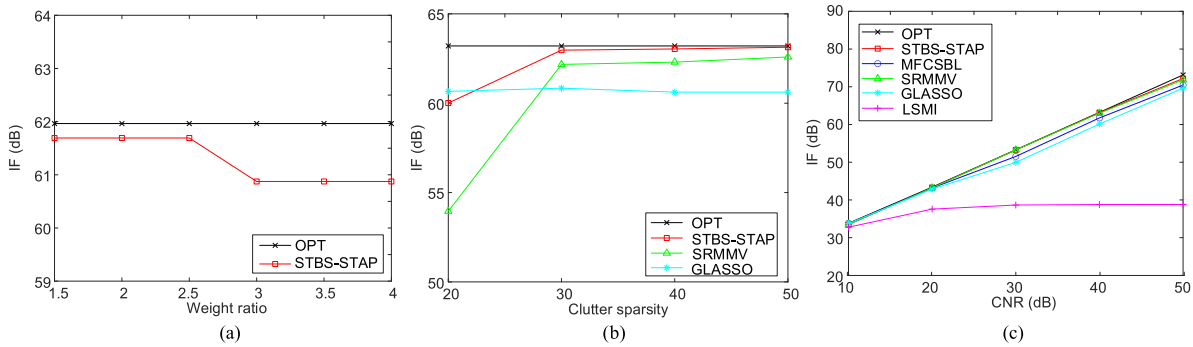

Fig. 6. IF curve in terms of (a) weight ratios in diagonal neighbors to those in nondiagonal neighbors (b) clutter sparsity (c) clutter-to-noise ratio. From (a), we find that the IF performance of STBS-STAP with weight ratios ranging from 1.5 to 2.5 is better than that when the weight ratio is ranging from 3 to 4. It is shown in (b) that the new STBS-STAP outperforms SRMMV and GLASSO when the clutter sparsity is larger than the true sparsity, i.e., around 30. From (c), we find that STBS-STAP achieves superior clutter suppression performance under different CNR scenarios.

TABLE I
RUNNING TIME OF DIFFERENT METHODS (S)

Methods	8 training samples		20 training samples	
	Parallel	Serial	Parallel	Serial
STBS-STAP	178.9	638.7	245.3	2156.0
SRMMV	114.2	581.6	151.4	1378.5
GLASSO	11.6	65.8	13.2	168.9
MFCSBL	-	460.6	-	586.3

better than that when the weight ratio is ranging from 3 to 4. The reason is that larger weight ratios means that we can obtain less information from nondiagonal neighbors. The information loss results in the performance degradation when weight ratio is too large. Therefore, we empirically set the ratio to be 2 as described in Section III-A. In Fig. 6(b), the IF values versus the clutter sparsity of different methods are demonstrated. Note that MFCSBL is independent on the parameter of the clutter sparsity and accordingly, the IF performance of MFCSBL is not included. Fig. 6(b) shows that STBS-STAP achieves better IF performance than SRMMV and GLASSO when the clutter sparsity is larger than the true sparsity, i.e., around 30. Besides, GLASSO exhibits robust performance to the clutter sparsity. In Fig. 6(c), the IF performances versus CNR of different methods are shown in the scenario. From Fig. 6(c), we find that the IF performance of STBS-STAP is close to the optimal case when CNR changes from 10 to 50 dB. SRMMV achieves similar IF performance to STBS-STAP. The IF values of MFCSBL and GLASSO are lower than STBS-STAP when CNR is 30–50 dB. In other words, STBS-STAP achieves superior clutter suppression performance when CNR varies. The reason is that the new STBS-STAP obtains more accurate estimation of the CCM by exploiting the property of the diagonal clustering structure and the common sparsity across the adjacent range cells, namely the STBS. In general, Fig. 6 proves again the superiority of STBS-STAP.

In the following, the running time of calculating CCM of different methods is given in Table I. Two operation modes are given in Table I, i.e., parallel computing and serial computing. The results are acquired by averaging from 50 Monte Carlo simulations in a computer environment with MATLAB 2019b, Intel Xeon platinum with 28 cores, 512GB RAM. From Table I, we find that the running time of STBS-STAP is slightly higher than that of SRMMV and MFCSBL with eight training samples in the mode of serial computing. The computational burden of STBS-STAP mainly results from SSCoSaMP(L1), which is utilized to acquire the initial support set corresponding to clutter area in step 1. The reason why we use SSCoSaMP(L1) here is that it exhibits superior performance when the sparse model with an overcomplete dictionary is observed [60]. The enforcement of STBS actually costs little computational resources. Though the running time is slightly higher, STBS-STAP achieves the better estimation of the clutter profile and better IF performance than MFCSBL, SRMMV, and GLASSO as shown in Figs. 4 and 5. Besides, the computational complexity of STBS-STAP increases linearly with the scale of the problem. Note that we can use the parallel computing toolbox of MATLAB to estimate the clutter profiles corresponding to each training sample in STBS-STAP, SRMMV, and GLASSO. The employment of the parallel computing reduces the running time at the cost of more computing resource. MFCSBL is designed to estimate the clutter profiles from multiple training samples collectively [25] and its computational cost cannot be further reduced by parallel computing. From Table I, we find that the running time of STBS-STAP is less than that of MFCSBL in the mode of parallel computing.

Moreover, MFCSBL yields much poorer detection performance than STBS-STAP with measured Mountain-Top data. In particular, the detection performance of STBS-STAP is 6.66dB higher than that of MFCSBL based on measured data when 12 training samples are available (more results can be found in the next subsection). GLASSO costs less time but achieves unsatisfactory IF performance. Though LSMI costs minimal time, it yields the worst IF performance. In general, it is acceptable to have a slightly higher computational burden according to the benefits obtained by STBS-STAP.

B. *Experimental Results on Measured Data*

In the following, the measured Mountain-Top data is utilized to compare the new STBS-STAP with existing state-of-the-art methods, such as, SRMMV, GLASSO, and MFCSBL. The

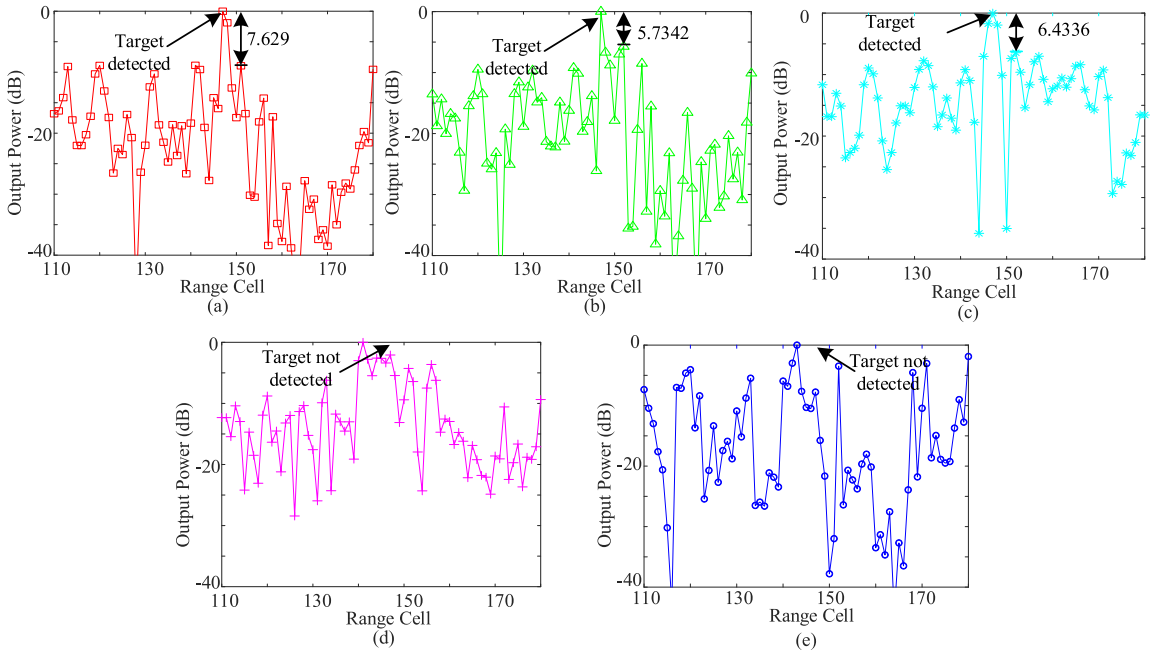

Fig. 7. Performance of (a) structure-aware two-level block sparsity-based space-time adaptive processing, (b) SRMMV, (c) group Lasso, (d) loaded sample matrix inversion, and (e) MFCSBL methods based on two training samples. The numbers in (a)–(c) indicate the output power difference between the detected target range cell with the largest output power and range cell with the second largest output power. The larger this difference is, the better the detection performance is. It is depicted in (a)–(e) that STBS-STAP achieves the better detection performance than SRMMV and GLASSO. In (d) and (e), the target is not detected because the target range cell does not have the largest output power.

Mountain-Top data is collected from a stationary multiple element array which is configured to emulate an airborne radar [63]. The radar system is composed of 14 elements and 16 pulses in one CPI. The target with the normalized Doppler frequency of 0.25 has been detected in the 147th range cell through preprocessing [64]. For STBS-STAP, we set the clutter sparsity to $K = 50$. The size of the block partition in GLASSO is 4. Other parameters are the same as the simulation part. The training snapshots are selected around the CUT, excluding four guard cells. For MFCSBL, the training sample selection strategy in [65] is employed according to [25].

Figs. 7 and 8 show the range detection performances of different approaches. The maximum value of each curve is normalized to 0 dB. The output power difference between the range cell corresponding to the detected target (which has the largest output power) and the range cell with the second largest output power is labeled in each subfigure. For the convenience of description, we simply refer to the above difference as the output power difference. Note that the performance on target detection is better if the output power difference is larger.

First, the range detection performances using two training samples are depicted in Fig. 7. We find the output power difference of STBS-STAP is larger than that of other methods even though the training samples are severely limited. This indicates that STBS-STAP achieves better performance on target detection and clutter suppression with a small number of training samples. Besides, GLASSO achieves the worse performance but still better than SRMMV. The target is not detected by using MFCSBL and LSMI due to severely lack of training snapshots.

TABLE II
DIFFERENCES BETWEEN OUTPUT POWER OF TARGET RANGE CELL AND NEXT HIGHEST POWER PEAK BASED ON MOUNTAIN-TOP DATA

Methods	2 training samples	12 training samples	22 training samples
STBS-STAP	7.6290dB	9.9094dB	11.5558dB
SRMMV	5.7342dB	3.4827dB	4.3603dB
GLASSO	6.4336dB	7.9635dB	8.1366dB
MFCSBL	-	3.2450dB	5.3604dB
LSMI	-	6.2197dB	7.4316dB

Next, we use 22 training samples to evaluate STBS-STAP and other methods in terms of the range detection performance as illustrated in Fig. 8. STBS-STAP also achieves the better target detection performance. The reason is that STBS-STAP employs multi-level information of the clutter, i.e., STBS. Accordingly, STBS-STAP acquires the accurate CCM estimation with limited training snapshots. On the contrary, the STAP methods based on SRMMV, GLASSO, and MFCSBL suffer from deteriorative performance due to the underutilization of block sparse information of clutter profiles, especially when the training snapshots are not enough. Specifically, we find that MFCSBL achieves poorer detection performance than the new STBS-STAP, e.g., the detection performance of MFCSBL is 6.19 dB lower than that of STBS-STAP with 22 training samples.

To compare these approaches distinctly, the output power difference results of three cases, i.e., $L = 2$, $L = 12$ and $L = 22$, are given in Table II. We can observe that as the quantity of training snapshots increase, the output power difference of each

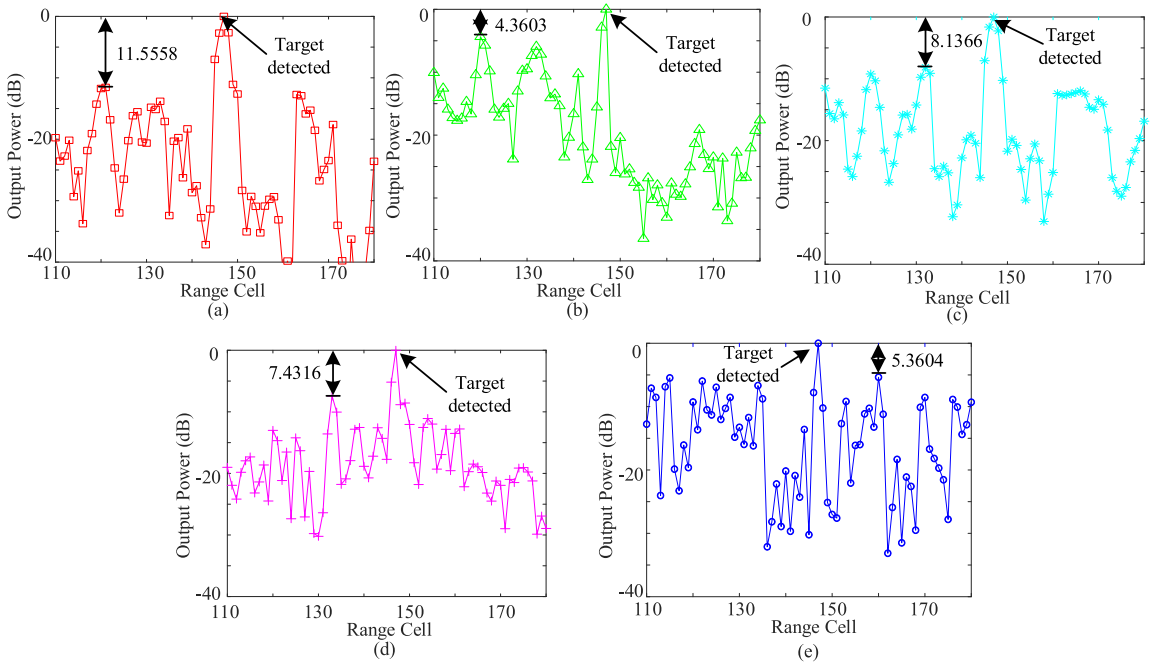

Fig. 8. Performance of of (a) structure-aware two-level block sparsity-based space-time adaptive processing, (b) SRMMV, (c) group Lasso, (d) loaded sample matrix inversion, and (e) MFCSBL methods based on 22 training samples. The numbers in (a)–(e) indicate the output power difference between the detected target range cell with the largest output power and range cell with the second largest output power. The larger this difference is, the better the detection performance is. It is depicted that STBS-STAP achieves the better detection performance than other methods.

method is improved except for SRMMV when $L = 2$. STBS-STAP achieves better detection performance than SRMMV and GLASSO in different situations. LSMI and MFCSBL do not detect the target using two training snapshots. All these results clearly illustrate that STBS-STAP achieves much superior performance on target detection and clutter suppression.

V. Conclusion

The performance on clutter suppression of conventional STAP degrades due to the inaccurate CCM estimation based on a small number of training snapshots.

In STAP applications, the clutter ridge presents a diagonal clustering structure in the angle-Doppler domain, it is a kind of special block sparse information of the clutter. Meanwhile, the clutter signals at the adjacent range cells commonly possess the same sparse pattern. It means the common sparsity of the clutter profiles is another kind of block sparsity.

In the article, we proposed a new STAP algorithm by utilizing STBS of the clutter component, namely STBS-STAP. In the new STBS-STAP, the underlying special diagonal clustering structure is captured by a MRF with the weighted eight-neighbor strategy. The smooth Gaussian function is modified to capture the contribution of the common sparsity. Then the diagonal clustering structure and the common sparsity are fused in STBS-STAP to acquire precise CCM estimation. As such, the combination of the special diagonal clustering structure and the common sparse pattern improves the performance on clutter suppression and target detection with a small number of training snapshots. Specifically, the employment of the special diagonal clustering structure reduces the required number of training snapshots. The utilization of the common sparsity eliminates the impact of the measurement noise.

Experimental results based on both the simulated data and measured Mountain-Top data show that the new STBS-STAP outperforms state-of-the-art sparsity-based STAP methods, such as SRMMV, GLASSO, and MFCSBL in terms of the performance on clutter suppression and target detection with the slight increase of computational complexity. Meanwhile, STBS-STAP achieves superior detection performance for targets that are close to the clutter ridge in the angle-Doppler domain. It signifies that STBS-STAP is promising in heterogeneous environments with a small number of training samples.

References

[1] L. Li, L. Du, and Z. Wang, "Target detection based on dual-domain sparse reconstruction saliency in SAR images," *IEEE J. Sel. Top Appl. Earth Observ. Remote Sens.,* vol. 11, no. 11, pp. 4230–4243, Oct. 2018.

[2] J. Liu, T. Jian, W. Liu, C. Hao, and D. Orlando, "Persymmetric adaptive detection with improved robustness to steering vector mismatches," *Signal Process,* vol. 176, pp. 1–10, May 2020.

[3] X. Chen, X. Yu, Y. Huang, and J. Guan, "Adaptive clutter suppression and detection algorithm for radar maneuvering target with high-order motions via sparse fractional ambiguity function," *IEEE J. Sel. Top Appl. Earth Observ. Remote Sens.,* vol. 13, pp. 1515–1526, Apr. 2020.

[4] J. W. Cheong, B. J. Southwell, and A. G. Dempster, "Blind sea clutter suppression for spaceborne GNSS-R target detection," *IEEE J. Sel. Top Appl. Earth Observ. Remote Sens.,* vol. 12, no. 12, pp. 5373–5378, Dec. 2019.

[5] Z. Jiang, G. Li, X. Wang, X.-P. Zhang, and Y. He, "STAP based on two-level block sparsity," in *Proc. IEEE Radar Conf.*, Apr. 2019, pp. 1–5.

[6] L. E. Brennan and L. S. Reed, "Theory of adaptive radar," *IEEE Trans. Aerosp. Electron. Syst.,* vol. AES-9, no. 2, pp. 237–252, Mar. 1973.

[7] J. Ward, *Space-Time Adaptive Processing For Airborne Radar*. Lincoln Labrotory, Mass. Inst. of Technology, Lexington, MA, USA, Tech. Rep. 1015, Dec. 1994.

[8] W. L. Melvin, "A STAP overview," *IEEE Aerosp. Electron. Syst. Mag.*, vol. 19, no. 1, pp. 19–35, Jan. 2004.

[9] J. Xu, G. Liao, and H. C. So, "Space-time adaptive processing with vertical frequency diverse array for range-ambiguous clutter suppression," *IEEE Trans. Geosci. Remote Sens.*, vol. 54, no. 9, pp. 5352–5364, Sep. 2016.

[10] E. Makhoul, S. V. Baumgartner, M. Jäger, and A. Broquetas, "Multichannel SAR-GMTI in maritime scenarios with F-SAR and TerraSAR-X sensors," *IEEE J. Sel. Top Appl. Earth Observ. Remote Sens.,* vol. 8, no. 11, pp. 5052–5067, Nov. 2015.

[11] S. D. Blunt, J. Metcalf, J. Jakabosky, J. Stiles, and B. Himed, "Multi-waveform space-time adaptive processing," *IEEE Trans. Aerosp. Electron. Syst.,* vol. 53, no. 1, pp. 385–404, Feb. 2017.

[12] S. Sen, "PAPR-constrained pareto-optimal waveform design for OFDM-STAP radar," *IEEE Trans. Geosci. Remote Sens.*, vol. 52, no. 6, pp. 3658–3669, Jun. 2014.

[13] R. Fa, R. C. de Lamare, and L. Wang, "Reduced-rank STAP schemes for airborne radar based on switched joint interpolation, decimation and filtering algorithm," *IEEE Trans. Signal Process.,* vol. 58, no. 8, pp. 4182–4194, Aug. 2010.

[14] A. B. C. d. Silva, S. V. Baumgartner, and G. Krieger, "Training data selection and update strategies for airborne post-doppler STAP," *IEEE Trans. Geosci. Remote Sens.*, vol. 57, no. 8, pp. 5626–5641, Aug. 2019.

[15] J. R. Guerci, *Space-Time Adaptive Processing For Radar*. Norwood, MA, USA: Artech House, 2003.

[16] B. D. Carlson, "Covariance matrix estimation errors and diagonal loading in adaptive arrays," *IEEE Trans. Aerosp. Electron. Syst.,* vol. 24, no. 4, pp. 397–401, Jul. 1988.

[17] C. H. Gierull, "Performance analysis of fast projections of the hung-turner type for adaptive beamforming," *Signal Process,* vol. 50, no. 1, pp. 17–28, Apr. 1996.

[18] M. L. Honig and J. S. Goldstein, "Adaptive reduced-rank interference suppression based on the multistage Wiener filter," *IEEE Trans. Commun.*, vol. 50, no. 6, pp. 986–994, Jun. 2002.

[19] S. Sen, "Low-rank matrix decomposition and spatio-temporal sparse recovery for STAP radar," *IEEE J. Sel. Top. Signal Process.*, vol. 9, no. 8, pp. 1510–1523, Dec. 2015.

[20] S. Sen, "OFDM radar space-time adaptive processing by exploiting spatio-temporal sparsity," *IEEE Trans. Signal Process.,* vol. 61, no. 1, pp. 118–130, Jan. 2013.

[21] Z. Wang, Y. Wang, F. Gao, and K. Duan, "Clutter nulling space-time adaptive processing algorithm based on sparse representation for airborne radar," *IET Radar Sonar Navigat.*, vol. 11, no. 1, pp. 177–184, May. 2017.

[22] M. Riedl and L. C. Potter, "Knowledge-aided bayesian space-time adaptive processing," *IEEE Trans. Aerosp. Electron. Syst.,* vol. 54, no. 4, pp. 1850–1861, Aug. 2018.

[23] X. Yang, Y. Sun, T. Zeng, T. Long, and T. K. Sarkar, "Fast STAP method based on PAST with sparse constraint for airborne phased array radar," *IEEE Trans. Signal Process.,* vol. 64, no. 17, pp. 4550–4561, Sep. 2016.

[24] Z. Yang, R. C. D. Lamare, and W. Liu, "Sparsity-based STAP using alternating direction method with gain/phase errors," *IEEE Trans. Aerosp. Electron. Syst.,* vol. 53, no. 6, pp. 2756–2768, Dec. 2017.

[25] Z. Wang, W. Xie, K. Duan, and Y. Wang, "Clutter suppression algorithm based on fast converging sparse bayesian learning for airborne radar," *Signal Process,* vol. 130, pp. 159–168, Jun. 2017.

[26] K. Duan, Z. Wang, W. Xie, H. Chen, and Y. Wang, "Sparsity-based STAP algorithm with multiple measurement vectors via sparse bayesian learning strategy for airborne radar," *IET Signal Process.*, vol. 11, no. 5, pp. 544–553, Jan. 2017.

[27] K. Sun, H. Meng, Y. Wang, and X. Wang, "Direct data domain STAP using sparse representation of clutter spectrum," *Signal Process.*, vol. 91, no. 9, pp. 2222–2236, Sep. 2011.

[28] S. F. Cotter, B. D. Rao, E. Kjersti, and K. Kreutz-Delgado, "Sparse solutions to linear inverse problems with multiple measurement vectors," *IEEE Trans. Signal Process.,* vol. 53, no. 7, pp. 2477–2488, Jul. 2005.

[29] K. Sun, H. Zhang, G. Li, H. Meng, and X. Wang, "A novel STAP algorithm using sparse recovery technique," in *Proc. IEEE Int. Geosci. Remote Sens. Symp.* 2009, vol. 5, pp. 336–339.

[30] K. Sun, H. Zhang, G. Li, H. Meng, and X. Wang, "Airborne radar STAP using sparse recovery of clutter spectrum," Aug. 2010. [Online]. Available: http://arxiv.org/abs/1008.4185

[31] M. Yuan and Y. Lin, "Model selection and estimation in regression with grouped variables," *J. Roy. Statist. Soc., B (Statist. Methodol.)*, vol. 68, no. 1, pp. 49–67. 2006.

[32] Y. C. Eldar, P. Kuppinger, and H. Bolcskei, "Block-sparse signals: Uncertainty relations and efficient recovery," *IEEE Trans. Signal Process.,* vol. 58, no. 6, pp. 3042–3054, Jun. 2010.

[33] M. G. Amin, B. Jokanovic, Y. D. Zhang, and F. Ahmad, "A sparsity-perspective to quadratic time–frequency distributions," *Digit. Signal Process.*, vol. 46, pp. 175–190, Nov. 2015.

[34] L. Wang, Y. Liu, Z. Ma, and H. Meng, "A novel STAP method based on structured sparse recovery of clutter spectrum," in *Proc. IEEE Radar Conf.*, May. 2015, pp. 561–565.

[35] L. Wang, L. Zhao, G. Bi, and C. Wan, "Hierarchical sparse signal recovery by variational Bayesian inference," *IEEE Signal Process. Lett.,* vol. 21, no. 1, pp. 110–113, Jan. 2014.

[36] Q. Wu, Y. D. Zhang, M. G. Amin, and B. Himed, "Multi-task Bayesian compressive sensing exploiting intra-task dependency," *IEEE Signal Process. Lett.,* vol. 22, no. 4, pp. 430–434, Apr. 2015.

[37] J. Liu, Q. Wu, and Y. D. Zhang, "Multi-task adaptive matching pursuit for sparse signal recovery exploiting signal structures," in *Proc. IEEE Int. Conf. Acoust., Speech, Signal Process.*, May 2019, pp. 4998–5002.

[38] X. Wang, G. Li, Y. Liu, and M. G. Amin, "Two-level block matching pursuit for polarimetric through-wall radar imaging," *IEEE Trans. Geosci. Remote Sens.*, vol. 56, no. 3, pp. 1533–1545, Mar. 2018.

[39] V. Cevher, M. Duarte, C. Hegde, and R. Baraniuk, "Sparse signal recovery using Markov random fields," in *Proc. Adv. Neural Inf. Process. Syst.*, 2009, pp. 257–264.

[40] W. Zhang, Z. S. He, and H. Y. Li, "Space time adaptive processing based on sparse recovery and clutter reconstructing," *IET Radar Sonar Navigat.*, vol. 13, no. 5, pp. 789–794, May. 2019.

[41] W. Zhang, R. An, N. He, Z. He, and H. Li, "Reduced dimension STAP based on sparse recovery in heterogeneous clutter environments," *IEEE Trans. Aerosp. Electron. Syst.,* vol. 56, no. 1, pp. 785–795, Feb. 2020.

[42] Y. Guo and J. Gong, "Direct data domain space-time adaptive processing method based on joint sparse representation with single snapshot for MIMO radar," *J. Appl. Remote Sens.*, vol. 14, no. 2, Jun. 2020, Art. no. 026522.

[43] X. Wang, Z. Yang, J. Huang, and R. C. D. Lamare, "Robust two-stage reduced-dimension sparsity-aware STAP for airborne radar with coprime arrays," *IEEE Trans. Signal Process.,* vol. 68, pp. 81–96, Dec. 2020.

[44] F. Tao, T. Wang, J. Wu, and Y. Su, "A knowledge aided SPICE space time adaptive processing method for airborne radar with conformal array," *Signal Process.*, vol. 152, pp. 54–62, Nov. 2018.

[45] T. Zhang, Y. Hu, and R. Lai, "Gridless super-resolution sparse recovery for non-sidelooking STAP using reweighted atomic norm minimization," *Multidimensional Syst. Signal Process.*, 2021.

[46] Z. Li, Y. Zhang, X. He, and Y. Guo, "Low-complexity off-grid STAP algorithm based on local search clutter subspace estimation," *IEEE Geosci. Remote Sens. Lett.,* vol. 15, no. 12, pp. 1862–1866, Dec. 2018.

[47] P. He, S. He, Z. Yang, and P. Huang, "An off-grid STAP algorithm based on local mesh splitting with bistatic radar system," *IEEE Signal Process. Lett.,* vol. 27, pp. 1355–1359, Jul. 2020.

[48] K. Duan, W. Liu, G. Duan, and Y. Wang, "Off-grid effects mitigation exploiting knowledge of the clutter ridge for sparse recovery STAP," *IET Radar Sonar Navig.*, vol. 12, no. 5, pp. 557–564. 2018.

[49] O. Kreyenkamp and R. Klemm, "Doppler compensation in forward-looking STAP radar," *IEE Radar Sonar Navig.,* vol. 148, no. 5, pp. 253–258, Oct. 2001.

[50] Z. Yang, R. C. d. Lamare, and X. Li, "L1-Regularized STAP algorithms with a generalized sidelobe canceler architecture for airborne radar," *IEEE Trans. Signal Process.,* vol. 60, no. 2, pp. 674–686, Feb. 2012.

[51] Q. Wu, Y. D. Zhang, M. G. Amin, and B. Himed, "Space-time adaptive processing and motion parameter estimation in multistatic passive radar using sparse bayesian learning," *IEEE Trans. Geosci. Remote Sens.*, vol. 54, no. 2, pp. 944–957, Feb. 2016.

[52] Z. Yang, X. Li, H. Wang, and W. Jiang, "On clutter sparsity analysis in space-time adaptive processing airborne radar," *IEEE Geosci. Remote Sens. Lett.,* vol. 10, no. 5, pp. 1214–1218, Sep. 2013.

[53] L. Wang, L. Zhao, G. Bi, and C. Wan, "Sparse representation-based ISAR imaging using Markov random fields," *IEEE J. Sel. Top Appl. Earth Observ. Remote Sens.,* vol. 8, no. 8, pp. 3941–3953, Aug. 2015.

[54] C. Gao, L. Wang, Y. Xiao, Q. Zhao, and D. Meng, "Infrared small-dim target detection based on Markov random field guided noise modeling," *Pattern Recognit.*, vol. 76, pp. 463–475, Apr. 2018.

[55] L. Wang, L. Zhao, G. Bi, C. Wan, and L. Yang, "Enhanced ISAR imaging by exploiting the continuity of the target scene," *IEEE Trans. Geosci. Remote Sens.*, vol. 52, no. 9, pp. 5736–5750, Sep. 2014.

[56] J. Zhang, "The mean field theory in EM procedures for Markov random fields," *IEEE Trans. Signal Process.,* vol. 40, no. 10, pp. 2570–2583, Oct. 1992.
[57] J. A. Tropp and A. C. Gilbert, "Signal recovery from random measurements via orthogonal matching pursuit," *IEEE Trans. Inf. Theory*, vol. 53, no. 12, pp. 4655–4666, Dec. 2007.
[58] V. Cevher, P. Indyk, L. Carin, and R. G. Baraniuk, "Sparse signal recovery and acquisition with graphical models," *IEEE Signal Process. Mag.*, vol. 27, no. 6, pp. 92–103, Nov. 2010.
[59] D. Koller and N. Friedman, *Probabilistic Graphical Models—Principles and Techniques*. Cambridge, MA, USA: MIT Press, 2009.
[60] M. A. Davenport, D. Needell, and M. B. Wakin, "Signal space CoSaMP for sparse recovery with redundant dictionaries," *IEEE Trans . Inf. Theory,* vol. 59, no. 10, pp. 6820–6829, Oct. 2013.
[61] D. Sundman, S. Chatterjee, and M. Skoglund, "Distributed greedy pursuit algorithms," *Signal Process.*, vol. 105, pp. 298–315, May. 2014.
[62] R. Klemm, *Principles of Space-Time Adaptive Processing*. London, U.K.: Inst. Eng. Technol., 2006.
[63] G. W. Titi and D. F. Marshall, "The ARPA/NAVY mountaintop program: Adaptive signal processing for airborne early warning radar," in *Proc. IEEE Int. Conf. Acoust., Speech, Signal Process.*, May 1996, pp. 1165–1168.
[64] S. Han, C. Fan, and X. Huang, "A novel STAP based on spectrum-aided reduced-dimension clutter sparse recovery," *IEEE Geosci. Remote Sens. Lett.,* vol. 14, no. 2, pp. 213–217, Feb. 2017.
[65] Y. Wu, T. Wang, J. Wu, and J. Duan, "Robust training samples selection algorithm based on spectral similarity for space–time adaptive processing in heterogeneous interference environments," *IET Radar Sonar Navig.*, vol. 9, no. 7, pp. 778–782, Oct. 2015.

Zhizhuo Jiang received the B.S. and M.S. degrees in electronic engineering from the Harbin Institute of Technology, Harbin, China, in 2014 and 2016, respectively. He is currently pursuing Ph.D. degree in electronic engineering with Tsinghua University, Beijing, China.

His main research interests include target detection, array signal processing, information fusion and compressed sensing.

Xueqian Wang (Member, IEEE) received the B.S. and Ph.D. degrees in electronic engineering from the University of Electronic Science and Technology of China, Chengdu, China, in 2015, and Tsinghua University, Beijing, China, in 2020, respectively.

He is currently a Post-Doctoral Fellow with the Department of Electronic Engineering, Tsinghua University, Beijing, China. From 2018 to 2019, he visited Syracuse University, Syracuse, NY, USA. His main research interests include target detection, information fusion, radar imaging, compressed sensing and distributed signal processing.

Gang Li (Senior Member, IEEE) received the B.S. and Ph.D. degrees in electronic engineering from Tsinghua University, Beijing, China, in 2002 and 2007, respectively.

Since July 2007, he has been with the Faculty of Tsinghua University, where he is currently a Professor with the Department of Electronic Engineering. From 2012 to 2014, he visited Ohio State University, Columbus, OH, USA, and Syracuse University, Syracuse, NY, USA. He has authored or coauthored more than 170 journal and conference papers. He is the Author of Advanced Sparsity-Driven Models and Methods for Radar Applications. His research interests include radar imaging, distributed signal processing, sparse signal processing, micro-Doppler analysis, and information fusion.

Dr. Li is currently an Associate Editor for the IEEE TRANSACTIONS ON SIGNAL PROCESSING.

Xiao-Ping Zhang (Fellow, IEEE) received B.S. and Ph.D. degrees in electronic engineering from Tsinghua University, in 1992 and 1996, respectively, and the MBA degree (Hons.) in finance, economics, and entrepreneurship with Honors from the University of Chicago Booth School of Business, Chicago, IL, USA.

Since Fall 2000, he has been with the Department of Electrical, Computer and Biomedical Engineering, Ryerson University, Toronto, ON, Canada, where he is currently a Professor and the Director of the Communication and Signal Processing Applications Laboratory. He has served as the Program Director of Graduate Studies. He is cross-appointed to the Finance Department at the Ted Rogers School of Management, Ryerson University. He was a Visiting Scientist with the Research Laboratory of Electronics, Massachusetts Institute of Technology, Cambridge, MA, USA, in 2015 and 2017. He is a Frequent Consultant for biotech companies and investment firms. His research interests include statistical signal processing, sensor networks and IoT, image and multimedia content analysis, machine learning, and applications in big data, finance, and marketing.

Dr. Zhang is a Fellow of the Canadian Academy of Engineering, a Fellow of the Engineering Institute of Canada, a Fellow of the IEEE, a registered Professional Engineer in Ontario, Canada, and a Member of Beta Gamma Sigma Honor Society. He is the General Co-Chair for the IEEE International Conference on Acoustics, Speech, and Signal Processing, 2021. He is the General Co-Chair for 2017 GlobalSIP Symposium on Signal and Information Processing for Finance and Business, and the General Co-Chair for 2019 GlobalSIP Symposium on Signal, Information Processing and AI for Finance and Business. He was an Elected Member of the ICME Steering Committee. He is the General Chair for the IEEE International Workshop on Multimedia Signal Processing, 2015. He is the Publicity Chair for the International Conference on Multimedia and Expo 2006, and the Program Chair for International Conference on Intelligent Computing in 2005 and 2010. He was a Guest Editor for the *Multimedia Tools and Applications* and the *International Journal of Semantic Computing*. He was a Tutorial Speaker at the 2011 ACM International Conference on Multimedia, the 2013 IEEE International Symposium on Circuits and Systems, the 2013 IEEE International Conference on Image Processing, the 2014 IEEE International Conference on Acoustics, Speech, and Signal Processing, the 2017 International Joint Conference on Neural Networks and the 2019 IEEE International Symposium on Circuits and Systems. He is a Senior Area Editor for the IEEE TRANSACTIONS ON IMAGE PROCESSING and the IEEE TRANSACTIONS ON SIGNAL PROCESSING. He was Associate Editor for the IEEE TRANSACTIONS ON IMAGE PROCESSING, the IEEE TRANSACTIONS ON MULTIMEDIA, the IEEE TRANSACTIONS ON CIRCUITS AND SYSTEMS FOR VIDEO TECHNOLOGY, the IEEE TRANSACTIONS ON SIGNAL PROCESSING, and the IEEE SIGNAL PROCESSING LETTERS. He was the recipient of 2020 Sarwan Sahota Ryerson Distinguished Scholar Award – the Ryerson University highest honor for scholarly, research and creative achievements. He is an IEEE Distinguished Lecturer by the IEEE Signal Processing Society for the term 2020 to 2021, and by the IEEE Circuits and Systems Society for the term 2021 to 2022.

You He received the Ph.D. degree in electronic engineering from Tsinghua University, Beijing, China, in 1997.

He is currently a Professor with Naval Aviation University, Yantai, China. He is also cross-appointed to the Department of Electronic Engineering, Tsinghua University. He has authored or coauthored 300 academic articles. He is the Author of Radar Target Detection and CFAR Processing (Tsinghua University Press) and Multisensor Information Fusion With Applications and Radar Data Processing With Applications (Publishing House of Electronics Industry). His current research interests include detection and estimation theory, CFAR processing, distributed detection theory, and multisensor information fusion.

Dr. He is also a Fellow Member of the Chinese Academy of Engineering. In 2017, he was a recipient of the Top Prize in Science and Technology of Shandong Province. He currently serves on the editorial boards for *the Journal of Data Acquisition and Processing*, *Modern Radar*, *Fire Control and Command Control*, and *Radar Science and Technology.*